Slug-expressing mouse prostate epithelial cells have increased stem cell potential

Zuzana Kahounová[a], Ján Remšík[a,b,c,1], Radek Fedr[a,b], Jan Bouchal[d], Alena Mičková[d], Eva Slabáková[a], Lucia Binó[a,2], Aleš Hampl[b,e], Karel Souček[a,b,c,*]

[a] *Institute of Biophysics of the Czech Academy of Sciences, Královopolská 135, 612 65 Brno, Czech Republic*
[b] *Center of Biomolecular and Cellular Engineering, International Clinical Research Center, St. Anne's University Hospital Brno, Pekařská 53, 656 91 Brno, Czech Republic*
[c] *Department of Experimental Biology, Faculty of Science, Masaryk University, Brno, Czech Republic*
[d] *Department of Clinical and Molecular Pathology, Institute of Molecular and Translational Medicine, Palacky University and University Hospital, Olomouc, Czech Republic*
[e] *Department of Histology and Embryology, Faculty of Medicine, Masaryk University, Brno, Czech Republic*

ARTICLE INFO

ABSTRACT

Deciphering the properties of adult stem cells is crucial for understanding of their role in healthy tissue and in cancer progression as well. Both stem cells and cancer stem cells have shown association with epithelial-to-mesenchymal transition (EMT) in various tissue types. Aiming to investigate the epithelial and mesenchymal phenotypic traits in adult mouse prostate, we sorted subpopulations of basal prostate stem cells (mPSCs) and assessed the expression levels of EMT regulators and markers with custom-designed gene expression array. The population of mPSCs defined by a Lin^-/Sca-$1^+$$CD49f^{hi}$/$Trop$-$2^+$ (LSC Trop-2^+) surface phenotype was enriched in mesenchymal markers, especially EMT master regulator Slug, encoded by the *Snai2* gene. To further dissect the role of Slug in mPSCs, we used transgenic Snai2$^{tm1.1Wbg}$ reporter mouse strain. Using this model, we confirmed the presence of mesenchymal traits and increase of organoid forming capacity in Slug$^+$ population of mPSCs. The Slug$^+$-derived organoids comprised all prostate epithelial cell types – basal, luminal, and neuroendocrine. Collectively, these data uncover the important role of Slug expression in the physiology of mouse prostate stem cells.

1. Introduction

Identification and proper characterization of adult stem cells within the prostate tissue is important for clarifying their role not only in tissue homeostasis and repair, but also in carcinogenesis.

Prostate epithelium is composed of three main epithelial cell types – basal, luminal, and neuroendocrine (NE) cells. The question of emergence of these cell types, whether from one common stem cell or multiple stem cells, is still not unequivocally answered, because different studies show that in mouse prostate, stem cells can reside within the population of both basal and luminal cells. Lee and colleagues identified 7 different subtypes of basal cells within mouse prostate and determined p63$^+$ basal cells as subpopulation containing adult stem cells, since this subpopulation was able to generate basal, luminal and NE cells also during prostate regeneration (Lee et al., 2014). Luminal cells were found to be derived from the basal layer and basal-derived

lineage is responsible for prostate development and tissue regeneration (Zhou et al., 2013). Goldstein *et al.* showed that subpopulation of mouse prostate basal cells with phenotype Lin^-/Sca-$1^+$$CD49f^{hi}$/$Trop2^+$ (LSC Trop-2^+) have stem cell characteristics (Goldstein et al., 2008). Later, Trop-2 was confirmed to regulate self-renewal, proliferation, and transformation in prostate cancer (Stoyanova et al., 2012). The origin of the rarest cell type, the NE cells, is still indefinite. There are two models describing the origin of these cells – common prostate stem cell as a origin of basal, luminal, and NE cells (Bonkhoff and Remberger, 1996), or model describing development of NE cells from neural crest (Szczyrba et al., 2017). By introducing a relevant organoid model, it was found out that both the basal and luminal mouse prostate cells can generate multilayer organoids (Karthaus et al., 2014).

Epithelial-to-mesenchymal transition (EMT) is a dynamic and plastic, evolutionarily conserved transcriptional program, during which epithelial cells turn into transient or permanent mesenchymal state.

Mesenchymal traits associate with increased motility and invasive properties (summarized in Zhang and Weinberg, 2018). Importantly, mechanistic dissection of the EMT program showed that EMT transcription factors are able to promote and maintain stemness, and induce tumorigenesis in several different tissue types (summarized in Lamouille et al., 2014).

In our work, we focused on the mouse prostate basal cells characterized by Lin$^-$/Sca-1$^+$CD49f^{hi}/Trop2$^+$ surface phenotype. To elucidate their EMT phenotype, we used mouse modeling, multicolor flow cytometry, gene expression analysis, immunohistochemistry, and organoid assays. We uncovered a partial mesenchymal phenotype of these cells with high expression of core EMT-inducing transcription factor *Snai2*/Slug.

2. Material and methods

2.1. Mouse prostate isolation and dissociation

Prostates were isolated from C57BL/6 male mice at least eight weeks old. Mice were obtained from the Laboratory Animal Breeding and Experimental Facility of the Faculty of Medicine, Masaryk University, Brno, Czech Republic. Prostates were microdissected and processed as described previously (Lukacs et al., 2010) with minor modifications. Papain Dissociation System (Worthington Biochemical Corp.) was used for enzymatic digestion. See Supplementary material and methods for details.

Transgenic mouse line Snai2$^{tm1.1Wbg}$ (Slug-YFP) was described previously and obtained as a generous gift from Prof. Robert A. Weinberg, Whitehead Institute, Massachusetts Institute of Technology, Cambridge. Expression of YFP in these mice is driven by endogenous promoter of Slug (Ye et al., 2015). Genotyping of mice was performed with primer sets as described (Ye et al., 2015). Since we did not observe any difference in the content of YFP$^+$ cells, prostates were collected from both heterozygous and homozygous males (Supplementary Fig. S2). All animal studies were performed according to the approval from The Czech Academy of Sciences (CAS), supervised by the local ethical committee of the Institute of Biophysics of the CAS and performed by certified individuals (ZK, LB, JR, KS).

To compare C57BL/6 and Slug-YFP models we performed immunohistochemical analysis of Slug expression in prostate cryosections for both models. Results were analysed by trained expert and no differences between these two models in terms of Slug expression were found (data not shown).

2.2. Immunophenotype analysis using flow cytometry

Single cell suspension was blocked with 1% BSA in PBS (20 min) at room temperature (RT) and stained with cocktail of primary antibodies or appropriate isotype controls diluted in washing/staining (WS) buffer (1% BSA/PBS/0.01% NaN$_3$). All antibodies and isotype controls used for staining are listed in Supplementary Table S1. When biotinylated primary antibody Trop-2 was used, cells after incubation with cocktail of primary antibodies including Trop-2 were washed with WS buffer and incubated with PE/Cy7-conjugated streptavidin. Finally, cells were washed with PBS and stained with LIVE/DEAD Fixable Dead Cell Stain Kit (Thermo Fisher Scientific), washed with PBS and resuspended in WS buffer for subsequent analysis. All incubations were performed for 20 min at 4 °C and in the dark. In case of sorting for subsequent RNA isolation and organoid assay seeding, all steps were performed aseptically in fume hood, and NaN$_3$-free WS buffer was used.

Immunophenotype analysis and cell sorting were performed using FACSAria II Sorp 4L system (BD Biosciences), equipped with five lasers (excitation wavelengths: 355, 405, 488, 561, and 640 nm, respectively). Dead cells, cell debris, doublets, and aggregates were excluded from analyses (see Supplementary Figs. S1 and S3 for full gating strategy). Gates were set using proper isotype controls, negative controls or fluorescence minus one controls (FMO) (Supplementary Figs. S1, S3). For setup of compensation matrix, following kits were used: BD™ CompBead Anti-Rat and Anti-Hamster Ig, κ /Negative Control Compensation Particles Set (552845, BD Biosciences), UltraComp eBeads (eBioscience), and ArC Amine Reactive Compensation Bead Kit (A10346, Thermo Fisher Scientific). Experiment measurements were performed using FACSDiva software (Version 6.1.3; BD Biosciences). Data analysis was performed using FlowJo LLC Data Analysis Software (Version 7.6.5, Tree Star). For sorting, cells were processed as described above, a 85- or 100-µm nozzle (20 psi) was used, and the sorting rate was no more than 1000 events per second. Gating strategies for sorting for particular experiments are shown in Supplementary Fig. S4. All data from flow cytometry experiments (isotype controls, specific stains) as well as examples of gating strategies from sorting experiments are available in FlowRepository (FR-FCM-Z2YL) (Spidlen et al., 2012).

2.3. Organoid assay

The 3D organoid assays were performed as described previously (Drost et al., 2016). Briefly, prostates from Slug-YFP mice were dissociated into single cell suspensions, stained for cell surface markers, and sorted as described in Section 2.1 and 2.2. Together 6 different subpopulations (each seeded in technical duplicate) from 3 mice were analyzed. Equal numbers of cells per phenotype (usually 1000–2000) were sorted directly into Cultrex® Reduced Growth Factor Basement Membrane Extract, type II, PathClear® (GFR BME, Trevigen), using continuously cooled microcentrifuge tube adapter. GFR BME was then mixed with complete organoid growth medium (75% of GFR BME in final volume) and a 40 µL drop containing 500 (2 mice) or 1000 (1 mouse) cells was placed into a centre of a well, in a 24 well plate. The drops were allowed to solidify at 37 °C for 30 min. Then, 1 mL of complete organoid medium was carefully added. See Supplementary material and methods for details. Data are presented as efficiency (%) of organoid formation, counted as number of organoids generated per well divided by the number of seeded cells.

2.4. Immunofluorescence analysis of organoids

The single cell suspensions from Slug-YFP prostates were obtained, processed and sorted as described in Sections 2.1 and 2.2. Organoid assay was performed as described in Section 2.3 with 500 cells seeded per well of 24 well plate. See Supplementary material and methods for details. All primary and secondary antibodies used for immunofluorescence analysis are listed in Supplementary Table S2. Images were acquired using Olympus FV10i confocal microscope, equipped with 60× objective. The resolution of raw images was 512 × 512px, 8× averaging, confocal aperture 2.0. Final image is stitched image of max. 16 FOVs. Insets were prepared using Fiji ImageJ software (Schindelin et al., 2012). Results presented in Fig. 5C are from multiple organoids generated by sorting of defined subpopulations of cells from one mouse prostate.

2.5. Standard and dual immunohistochemistry (IHC) of mouse prostate

Dissected prostates were mounted in Tissue-Tek® O.C.T.™ Compound (Sakura) and cryopreserved. Mouse tissue cryosections were fixed with 4% formaldehyde for 30 min. In the standard immunohistochemistry protocol, the primary antibodies were visualized using the Dako REAL EnVision Detection System, Peroxidase/DAB+, Rabbit/Mouse (Agilent). Following primary antibodies were used: E-cadherin, α-smooth muscle actin, and Slug. Dual staining was performed with Opal Multiplex Immunohistochemistry Kit (Perkin Elmer), according to the manufacturer's protocol. Briefly, the sections were first stained with anti-p63 antibody, EnVision HRP Rabbit/Mouse secondary antibody and Cyanine 5 tyramide. The staining procedure was repeated with anti-Slug and Cyanine 3 tyramide and nuclei were stained with

4′,6-diamidino-2-phenylindole (DAPI). Images were captured with the confocal microscope LSM 780 (Zeiss). Used antibodies are listed in Supplementary Table S3.

2.6. RNA isolation, cDNA synthesis, and qPCR analysis

For quantitative PCR (qPCR) analysis, 20 000 to 200 000 of cells defined by the following cell surface phenotypes were sorted directly into the tubes containing 1% BSA in PBS - Lin^-/Sca-1^+CD49f^{hi}/Trop-2^+ (LSC Trop-2^+) and non-mPSCs Lin^-/Sca-1^-/CD49f$^-$ (LSC$^-$), or Lin^-/Sca-1^+CD49f^{hi}/Slug-YFP$^+$ (LSC Slug-YFP$^+$) and Lin^-/Sca-1^+/CD49f^{hi}/Slug-YFP$^-$ (LSC Slug-YFP$^-$), respectively. After centrifugation (300g, 5 min), the pellets were lysed in lysis buffer and stored at -80 °C. Total RNA was isolated using High Pure RNA Isolation Kit (Roche). cDNA synthesis was performed in 50 μL reactions using Transcriptor High Fidelity cDNA synthesis Kit (Roche) according to manufacturer's recommendations. qPCR analysis was performed using 384-well platform RealTime Ready Custom Panel (Roche) using LightCycler 480 thermal cycler (Roche) with following profile: pre-incubation 95 °C 10 min; amplification: 95 °C 10 s, 60 °C 30 s, 72 °C 1 s (acquisition), 45–55 cycles; cooling 40 °C 30 s. Plates contained 3 reference genes, at least 2 were used for normalisation – β-actin (*Actb*), glyceraldehyde-3-phosphate dehydrogenase (*Gapdh*), or TATA box binding protein (*Tbp*). Used primers are listed in Supplementary Table S4. Data presented as relative gene expression were analyzed using $2_T^{-\Delta\Delta C}$ method (Livak and Schmittgen, 2001).

2.7. Data and statistical analysis

Images were processed with ImageJ. Data were plotted and statistical analyses were performed in Prism (GraphPad Software, Inc., version 8.0.2) using *t*-test. Heatmaps were plotted using Morpheus (Broad Institute).

3. Results

3.1. LSC Trop-2^+ mPSCs display partial mesenchymal phenotype

The connection between stem cell phenotype and EMT was previously described in numerous tissue types. To assess this in the adult prostate, we focused on the basal stem cell population of mouse prostate epithelium, characterized by the LSC Trop-2^+ cell surface phenotype. The mouse prostates from wild-type or Snai2$^{tm1.1Wbg}$ transgenic animals were dissociated into single-cell suspensions, sorted using multicolor cytometric approaches, and assayed by qPCR and organoid assays (Fig. 1A).

We sorted LSC Trop-2^+ (Lin^-/Sca-1^+CD49f^{hi}/Trop-2^+) mPSCs and LSC$^-$ (Lin^-/Sca-1^-CD49f$^-$) non-mPSCs (Fig. 1B, Supplementary Fig. S1 and S4A) and analyzed their expression of EMT regulators and markers using a custom gene expression array. We observed a significantly increased level of typical EMT regulator *Snai2* in LSC Trop-2^+ (Fig. 1C). *Axl*, another EMT regulator, was also increased, whereas *Twist1* and *Zeb1* were significantly downregulated in LSC Trop-2^+ cells. When EMT markers were analyzed in LSC Trop-2^+ subpopulation, lower level of mesenchymal markers vimentin (*Vim*) and fibronectin (*Fn1*), and no differences in level of epithelial marker E-cadherin (*Cdh1*) were detected (Fig. 1C). Only a trend towards increased expression of another mesenchymal marker α-smooth muscle actin (*Acta2*) was observed.

We further investigated levels of stem cell markers in LSC Trop-2^+ cells (Fig. 1D). Only an increased level of *Sox2* in LSC Trop-2^+ in comparison to LSC$^-$ was detected. We did not detect transcripts for *Oct4* and *Nanog* by our assay. We also analyzed expression of CD44, CD117 and Prominin-1 (CD133), since next to basal stem cells, presence of luminal stem cells with phenotype Lin^-/Sca-1^+/CD44$^+$/Prom-1^+/CD117$^+$ (LS CD117$^+$) was described in mouse prostate (Leong et al.,

2008). Only *Cd44* level was higher in LSC Trop-2^+ cells, whereas *Kit* and *Prom1* (genes encoding CD117 and Prominin-1, respectively) transcripts were significantly decreased in LSC Trop-2^+ cells. These results indicate that mPSCs with phenotype LSC Trop-2^+ and with phenotype LS CD117$^+$ define non-overlapping subpopulations within the mouse prostate.

In summary, screening of expression of numerous EMT markers and regulators uncovered significantly increased expression of Slug, core EMT transcription factor, in LSC Trop-2^+ cells. This indicates the presence of mesenchymal traits in LSC Trop-2^+ mPSCs.

3.2. LSC Trop-2^+ subpopulation express Slug protein

The expression of transcription factors is usually very low, thus their detection is often difficult. Using multicolor flow cytometry and fluorescent-conjugated primary antibodies we were not able to detect Slug on protein level in LSC Trop-2^+ cells. Therefore, to confirm the elevated Slug expression in LSC Trop-2^+ mPSCs using an alternative approach that would reflect the protein levels, we employed the model of transgenic Slug-YFP mice, where the expression of fluorescent tag YFP is driven by the endogenous *Snai2*/Slug promoter (Ye et al., 2015).

LSC Trop-2^+ subpopulation was particularly enriched in YFP$^+$ cells, in comparison to LSC$^-$ cells (Fig. 2A and Supplementary Fig. S3), which is in concordance with gene expression results from C57BL/6 mice. (Fig. 1C). Next we analyzed expressions of Sca-1, CD49f and Trop-2 in Lin^-/Slug-YFP$^+$ and Lin^-/Slug-YFP$^-$ subpopulations. As shown in Fig. 2B, YFP-positive cells were mostly Sca-1^+/CD49f^{hi} or Trop-2^+, when compared to YFP-negative cells. To assess the full spectrum of stem cell and EMT regulators, we sorted LSC YFP$^-$ (Lin^-/Sca-1^+CD49f^{hi}/Slug-YFP$^-$) and LSC YFP$^+$ (Lin^-/Sca-1^+CD49f^{hi}/Slug-YFP$^+$) cells (Supplementary Figure S4B) and compared their gene expression profiles using the gene expression array used above. Similarly to the findings in C57BL/6 mice (Fig. 1C), we detected increased levels of mesenchymal regulators *Axl* and *Slug* in LSC YFP$^+$ cells (Fig. 2C).

We were aware of the fact that there can be discrepancies in changes in RNA levels and protein levels of EMT markers and regulators, therefore we investigated protein levels of epithelial marker E-cadherin, mesenchymal marker α-smooth muscle actin, and Slug using IHC staining of mouse prostate in both C57BL/6 and Slug-YFP mice (Fig. 3). We found out that in prostates from both C57BL/6 and Slug-YFP mice, there are areas with weaker E-cadherin staining and concomitant Slug nuclear localisation (Fig. 3A), and areas with intense E-cadherin staining and concomitant Slug perinuclear/cytoplasmic localisation (Fig. 3B). These results support our finding that cells with expressing Slug are at least in partial mesenchymal state.

Altogether, we confirmed the presence of Slug protein in LSC Trop-2^+ cells and proved the validity and specificity of this approach using the analysis of wide array of EMT and stem cell regulators in sorted cellular fractions of mouse prostate from Slug-YFP transgenic animals.

3.3. Co-expression of Slug and p63 in mouse prostate basal cells

We further wanted to confirm that Slug is expressed in prostate basal cells. We performed cryosectioning of both C57BL/6 and Slug-YFP mouse prostate and stained these sections for Slug and prostate basal cell marker p63, as p63$^+$ basal cells were shown to contain adult stem cells (Lee et al., 2014). As shown in Fig. 4, we detect several cells co-expressing Slug and p63 in both C57BL/6 and Slug-YFP mouse prostate cryosections.

3.4. Slug expression is associated with increased propensity to form organoids

The expression of Slug in a specific subset of adult mouse prostate epithelial stem cells shown here suggested that Slug may promote or maintain the stemness of these cells. Intrigued by this observation, we
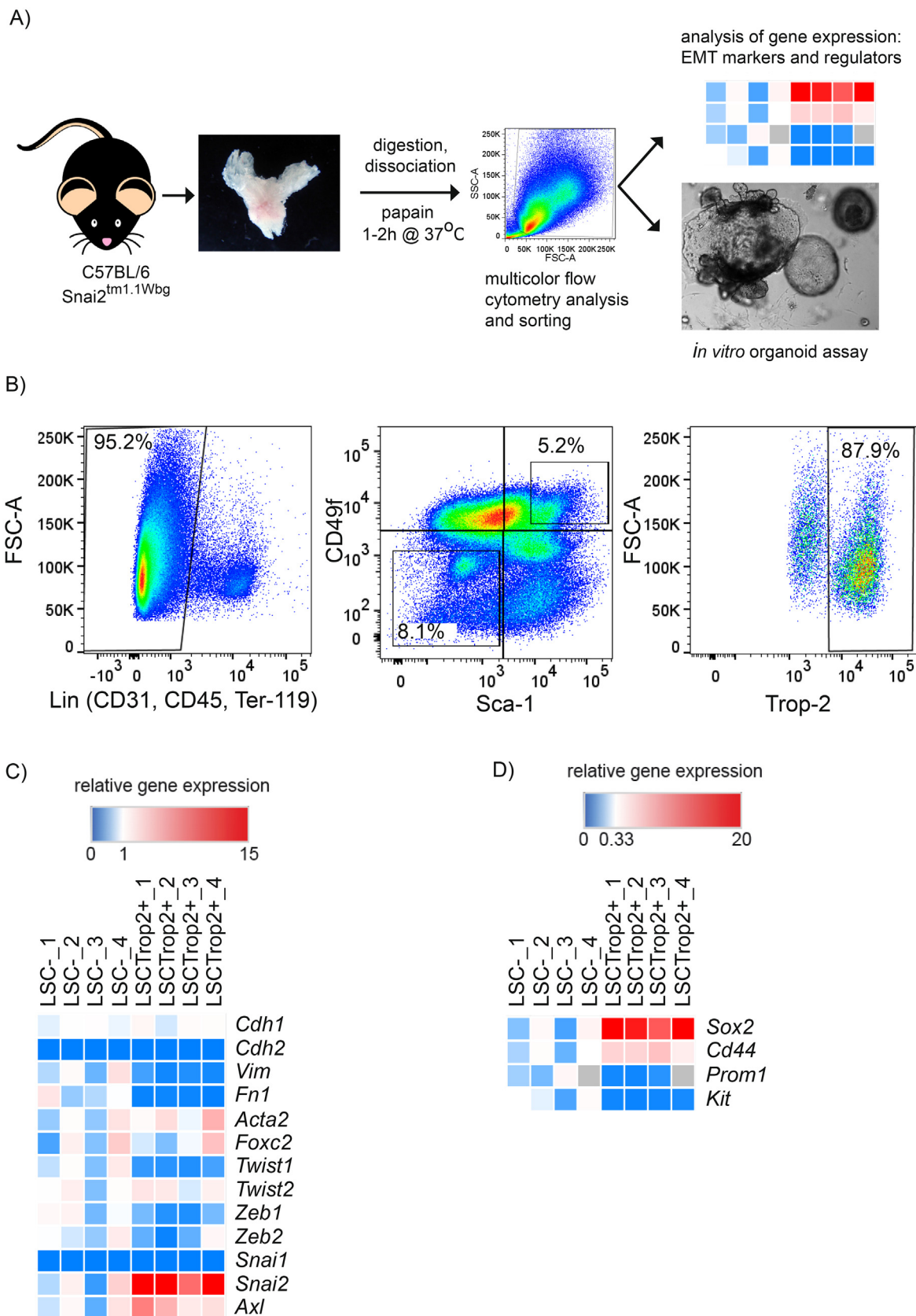
Fig. 1. LSC Trop-2⁺ mPSCs display partial mesenchymal phenotype with upregulated *Snai2/Slug.* A) Schematic workflow of experiments presented in this study. B) Identification of the mPSCs with LSC Trop-2⁺ cell surface phenotype. Full gating strategy and appropriate isotype control are shown in the Supplementary Fig. S1. C) Expression of EMT markers and regulators in the LSC Trop-2⁺ vs. LSC⁻ subpopulations, as detected by the qPCR analysis. Results are presented as heat maps of relative gene expression from four independent repetitions. D) Expression of stem cell markers in LSC Trop-2⁺ vs. LSC⁻ subpopulations detected by the qPCR. Results are presented as heat maps of relative gene expression from four independent repetitions. *Cdh1*, E-cadherin; *Cdh2*, N-cadherin; *Vim*, vimentin; *Fn1*, fibronectin 1; *Acta2*, α-smooth muscle actin; *Foxc2*, forkhead box protein 2; *Snai1*, Snail; *Snai2*, Slug; *Prom1*, Prominin-1; *Kit*, CD117; *Cd44*, CD44; *Sox2*, Sox 2.
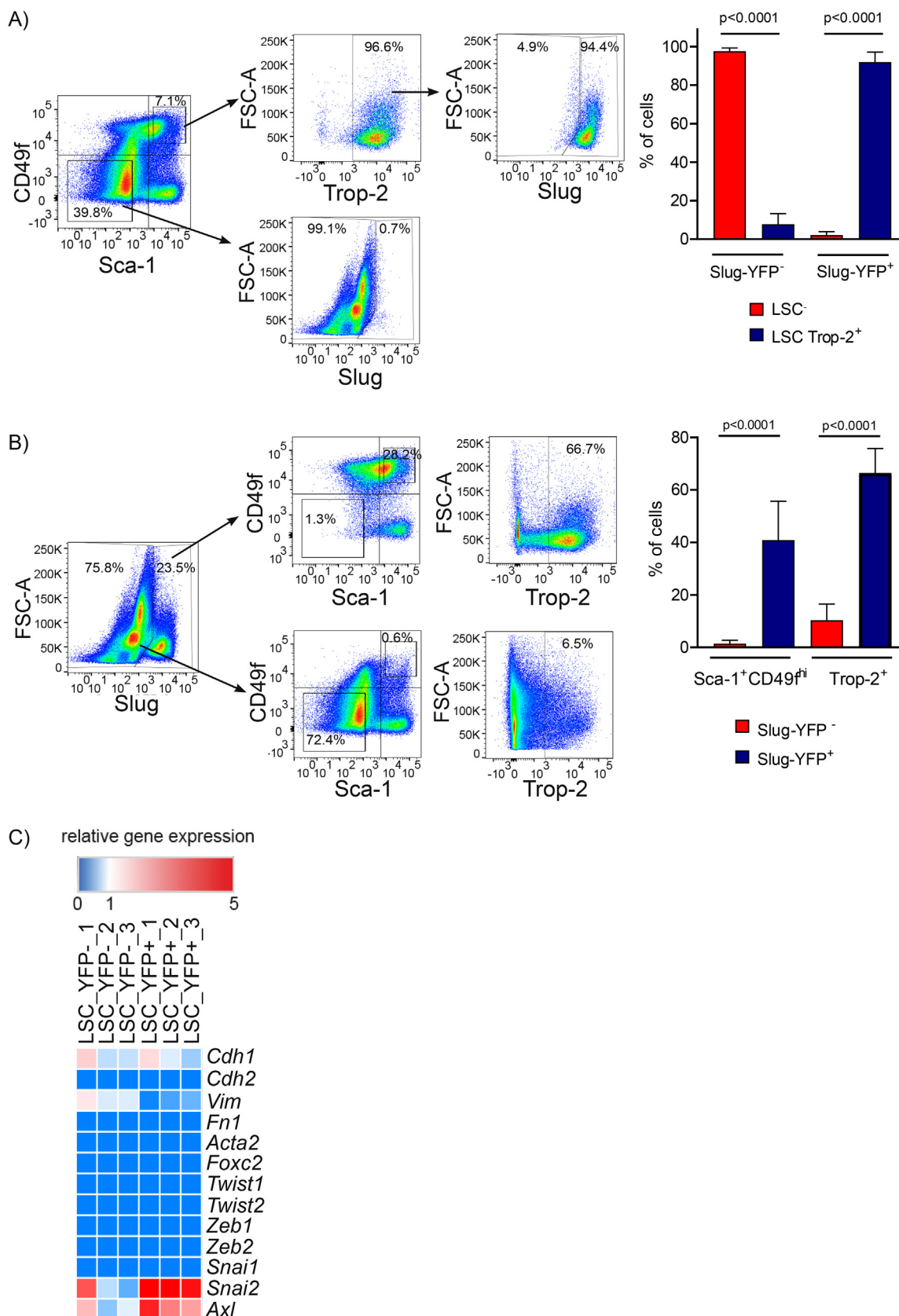
Fig. 2. LSC Trop-2$^+$ subpopulation express Slug protein. A) Quantification of Slug-YFP$^+$ cells in LSC Trop-2$^+$ cells, derived from Snai2$^{tm1.1Wbg}$ mice. Full gating strategy and isotype control are shown in the Supplementary Fig. S3. Graph shows results from six independent repetitions presented as mean ± S.D. B) Analysis of expression of Sca-1$^+$CD49f^{hi} and Trop-2$^+$ in Lin$^-$/Slug-YFP positive and negative cells. Graph shows results from six independent repetitions presented as mean ± S.D. C) qPCR analysis of EMT phenotype in sorted LSC Slug-YFP$^-$ vs. LSC Slug-YFP$^+$ cells. Results are presented as heat maps of relative gene expression from three independent repetitions.
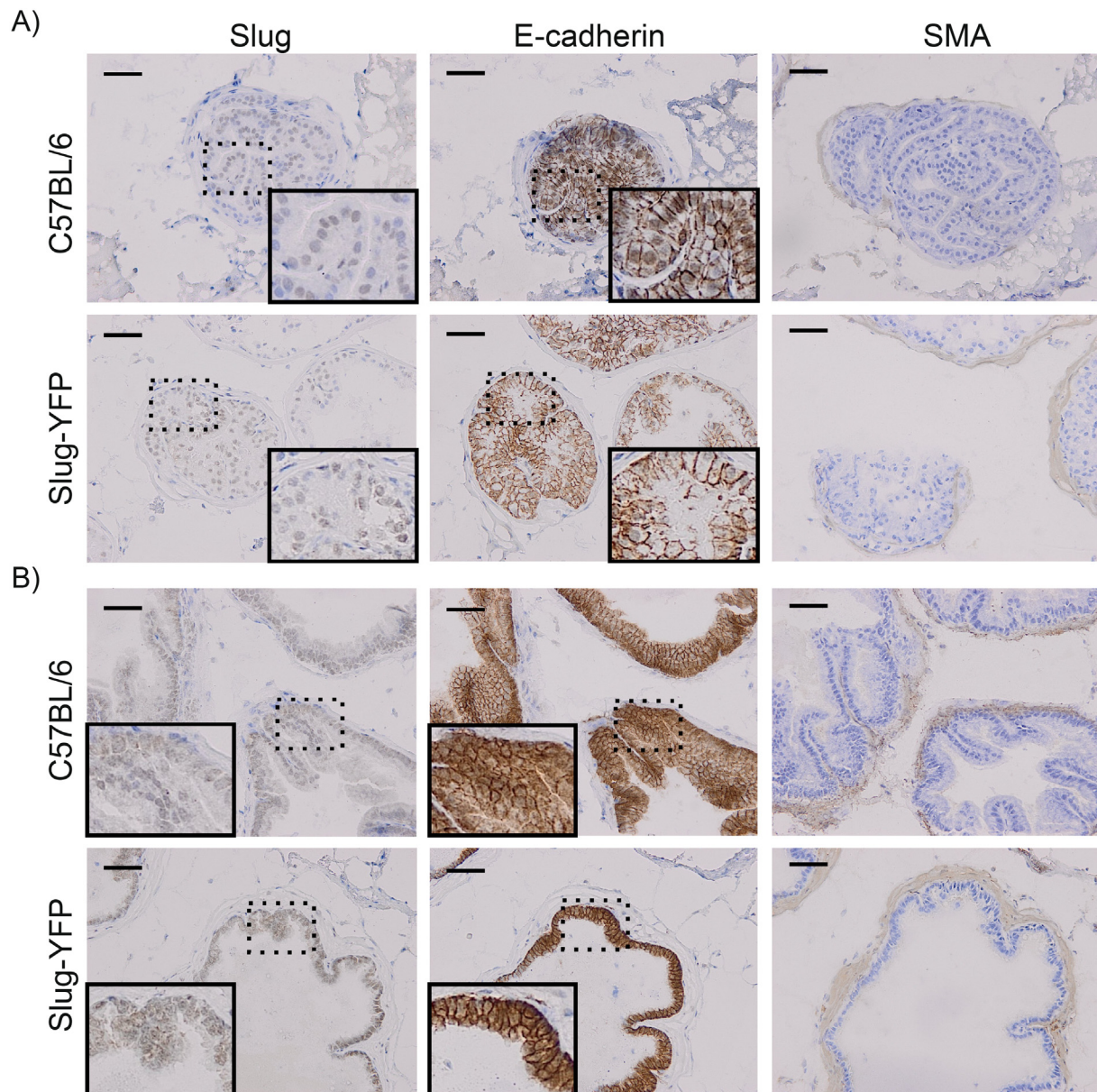
Fig. 3. Slug expression inversely correlate with E-cadherin in mouse prostate tissue sections. Analysis of epithelial marker E-cadherin, mesenchymal marker α-smooth muscle actin (SMA), and EMT regulator Slug in prostate cryosections from C57BL/6 and Slug-YFP mice. A) Areas, where weaker expression of E-cadherin correlates with nuclear Slug expression. B) Areas, where stronger expression of E-cadherin correlates with perinuclear/cytoplasmic localisation of Slug. α-smooth muscle actin was detected only in stromal compartments, not in epithelial cells. Representative reconcilable structures from C57BL/6 and Slug-YFP mouse prostates chosen for presentation. Magnification 200×. Scale bar 50 μm.

assayed the organoid forming capacity of sorted subpopulations differing in Slug expression (Fig. 5A and Supplementary Fig. S4C). As expected, expression of YFP, surrogating the protein expression of Slug, was associated with increased ability to form organoids.

Finally, we were interested in answering the question, whether the cells expressing Slug are able to generate all three epithelial prostate cell types - basal, luminal, and neuroendocrine. We stained the organoids formed by Lin$^-$/YFP$^+$ cells (Fig. 5B and Supplementary Fig. S4D) for typical lineage markers. As shown in Fig. 5C, organoids contained basal cells expressing keratin 8 (CK8) and p63, luminal cells expressing keratin 5 (CK5) and androgen receptor (AR), and rare neuroendocrine cells expressing synaptophysin (SYP).

In summary, using transgenic mouse model we confirmed high expression of Slug in LSC Trop2$^+$ cells in comparison to LSC$^-$ cells also on protein level, and also showed importance of Slug for stemness in organoid assay.

4. Discussion

Epithelial-to-mesenchymal transition is a developmental process, during which the epithelial cells acquire more mesenchymal phenotype associated with increased motility and invasiveness (summarized in Zhang and Weinberg, 2018). This highly dynamic and plastic process is reactivated during tumor progression. Induction of EMT in the mouse mammary epithelial cells leads to the acquisition of stem-like properties in these cells (Mani et al., 2008). Connection between EMT and prostate cancer stem cells was also described (Kong et al., 2010). As such, the induction of EMT and emergence of stem-like properties are interconnected in a variety of epithelial tissues. Therefore, here we assessed the epithelial-mesenchymal and stem cell traits in the adult mouse prostate basal epithelium, and we report that LSC Trop-2$^+$ mouse prostate basal stem cells have partially mesenchymal phenotype with high expression of Slug, a core EMT transcription factor.
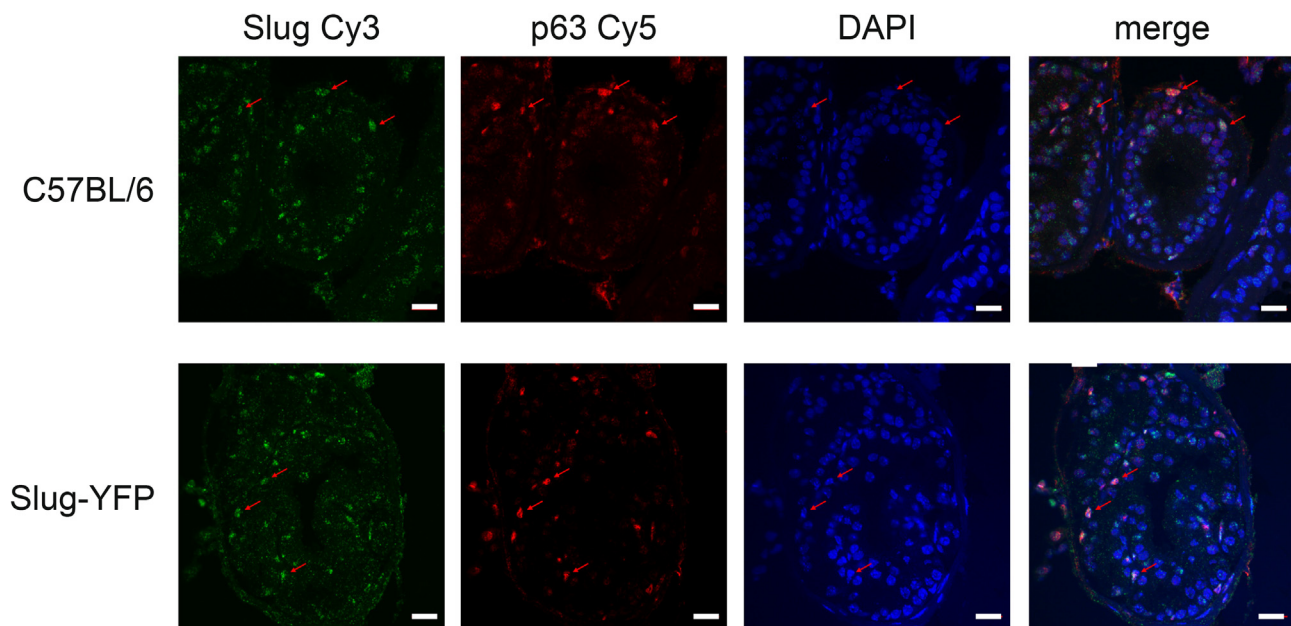
Fig. 4. Slug colocalize with p63 in both C57BL/6 and Slug-YFP prostate tissue. Prostate cryosections were analysed for Slug expression in basal cells expressing p63. Cells co-expressing Slug and p63 (indicated by arrow) were detected in both C57BL/6 and Slug-YFP prostate epithelium. Scale bar 20 μm.

In the prostate, similarly to other tissues, EMT was found to be essential process occurring during the development, as well as during carcinogenesis (summarized in Grant and Kyprianou, 2013). We therefore investigated the epithelial-mesenchymal phenotype of LSC Trop-2$^+$ cells. Using the robust combination of multicolor flow cytometry, cell sorting and qPCR, we unraveled that the LSC Trop-2$^+$ cells did not manifest purely epithelial or mesenchymal phenotype. Besides the detection of high enrichment of EMT regulators Slug and Axl in the LSC Trop-2$^+$ cells, we also observed low levels in some other EMT markers, such as Vimentin, Fibronectin, Twist1 or Zeb1. This confirms the previous observations that *in vivo* EMT is a highly dynamic process and that both normal and neoplastic cells rarely display marks of fully mesenchymal state, when EMT program is induced. This is further mirrored in the co-expression of both epithelial and mesenchymal markers, and described as partially epithelial or partially mesenchymal state (summarized in Nieto et al., 2016). Such intermediate states are likely dependent on the present equilibrium of transcriptional drivers and suppressors of EMT. As such, cells in these intermediate states were detected during developmental processes (Futterman et al., 2011), in tumor buds (summarized in Grigore et al., 2016), or in breast cancer circulating tumor cells (Yu et al., 2013).

Using qPCR, we detected no changes in the level of epithelial marker E-cadherin between LSC Trop-2$^+$ cells and LSC$^-$ cells. We are aware of the fact that although there are no changes on mRNA level, there may be changes on protein level of this epithelial marker, as was described previously (Hu et al., 2017). Therefore, we detected epithelial marker E-cadherin, mesenchymal marker α-smooth muscle actin, and Slug protein levels using IHC staining of mouse prostate cryo-samples in both C57BL/6 and Slug-YFP mice (Fig. 3). We found out that in prostates from both C57BL/6 and Slug-YFP mice, there are areas with weaker E-cadherin staining and concomitant Slug nuclear localisation (Fig. 3A), and areas with intense E-cadherin staining and concomitant Slug perinuclear/cytoplasmic localisation (Fig. 3B). These results support our finding that cells expressing Slug are at least in partial mesenchymal state.

To confirm Slug expression in prostate basal stem/progenitor cells, we performed co-staining of Slug and p63 (Fig. 4). p63 expressing cells in the developing prostate represent progenitor cells and p63$^+$ subpopulation contain adult basal stem cells (Signoretti et al., 2000). Our results show coexpression of Slug and p63 in several cells in both C57BL/6 and Slug-YFP prostates.

Slug, which belongs to the SNAIL superfamily of zinc finger proteins, is an important master transcription factor driving EMT through repression of epithelial E-cadherin (Bolos et al., 2003). We further confirmed the unusually high levels of Slug gene expression using Snai2$^{tm1.1Wbg}$ transgenic reporter mice, as a surrogate for protein levels due to the low abundance of this protein in the cell nucleus in general. The role of Slug in stem cells was previously shown in mammary tissue, where co-expression of Slug together with Sox9 led to the conversion of differentiated luminal cells into mammary stem cells (Guo et al., 2012). In the prostate, EMT phenotype of prostate basal cells with increased Slug expression was described in human benign tissue samples (Zhang et al., 2016). Slug also plays crucial physiological role during the mammary gland development, particularly in morphogenesis, mammary cell proliferation, differentiation, migration and apoptosis (Nassour et al., 2012). Moreover, distinct EMT programs were found to be governed by the Slug and Snail transcription factors in the mammary gland (Ye et al., 2015). While Slug drives partial EMT phenotype in normal mammary epithelial stem cells, manifested by mixed epithelial-mesenchymal phenotype, Snail induces purely mesenchymal state of mammary epithelial cells and drove cancer progression. In conclusion, the master EMT regulators are not redundant in terms of potency of EMT induction, and they are involved in EMT induction in different contexts.

Finally, we confirmed the functional relevance of Slug expression in LSC Trop-2$^+$ mPSCs using organoid assay. Organoids are defined as the *in vitro* 3D cellular clusters derived exclusively from primary tissues, embryonic stem cells and/or induced pluripotent stem cells, that are capable of self-renewal and self-organization, and exhibiting similar organ functionality as the tissue of origin (Fatehullah et al., 2016). Organoid structures are similar to their original tissue in terms of composition and organization. Karthaus *et al.* previously showed that both basal and luminal human prostate cells can give rise to organoids, but only luminal cell-derived organoids had branching morphology, resembling normal prostate gland architecture (Karthaus et al., 2014). In our hands, Slug expression associated with significantly higher ability to form organoids, and the organoids generated from Slug-expressing cells contained all three prostate cell types – basal cells, luminal cells, and neuroendocrine cells.

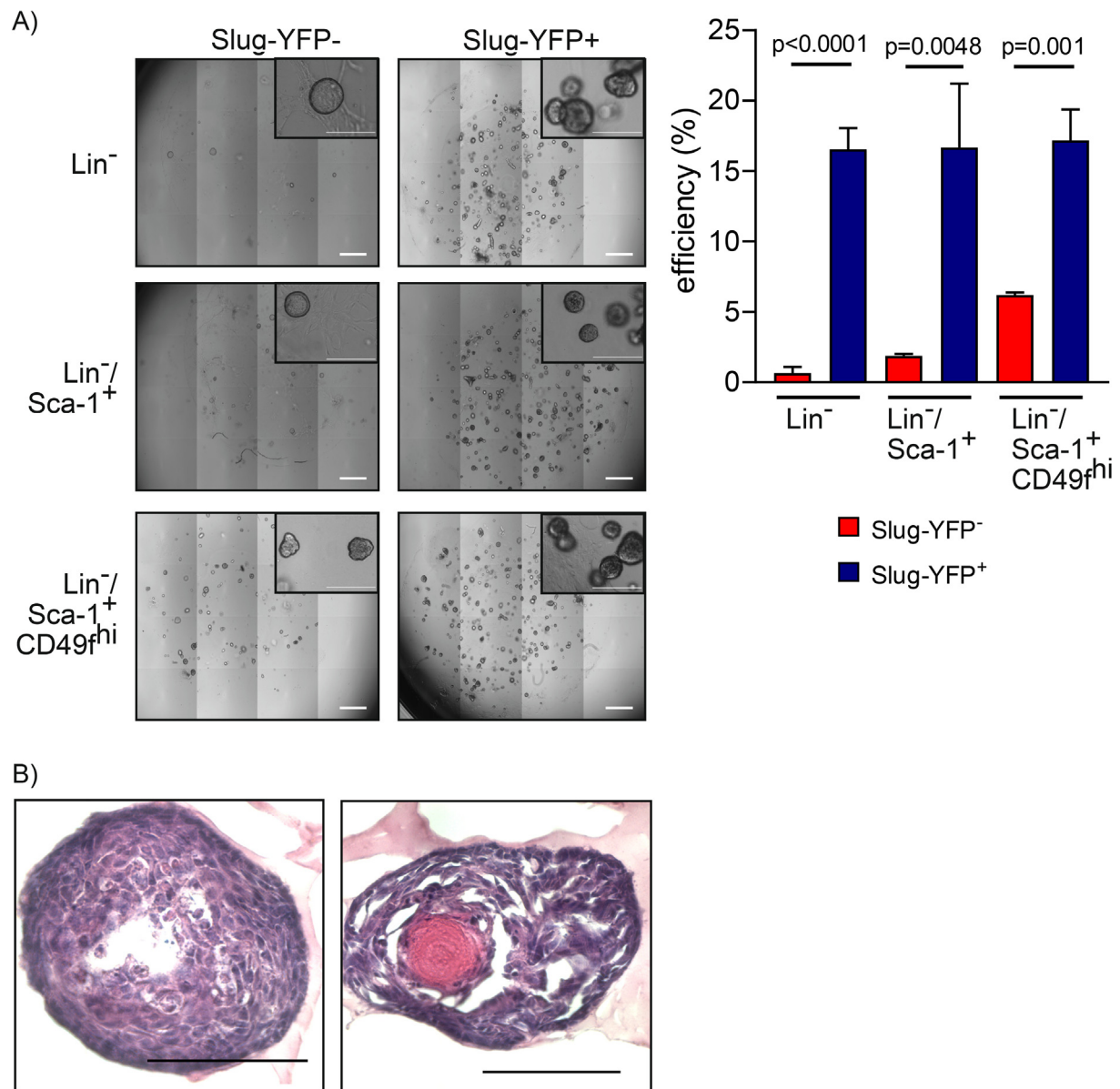In summary, we provide evidence that the Lin$^-$/Sca-1$^+$CD49f^{hi}/

Fig. 5. Slug expression is associated with increased ability to form organoids. A) Quantification of organoid assay. Sorted subpopulations Lin$^-$/Slug-YFP$^-$ vs. Lin$^-$/Slug-YFP$^+$, Lin$^-$/Sca-1$^+$/Slug-YFP$^-$ vs. Lin$^-$/Sca-1$^+$/Slug-YFP$^+$, and Lin$^-$/Sca-1$^+$CD49f^{hi}/Slug-YFP$^-$ vs. Lin$^-$/Sca-1$^+$CD49f^{hi}/Slug-YFP$^+$ were compared. Results are presented as mean efficiency of organoids formation $\pm$ S.D. from three independent repetitions performed in technical duplicate. Scale bar 1 mm, scale bar in inset 300 μm. B) Hematoxylin and eosin staining of organoids generated by sorted Lin$^-$/Slug-YFP$^+$ cells. Scale bar 50 μm. C) Immunofluorescence analysis of organoids generated by sorted Lin$^-$/Slug-YFP$^+$ cells. Markers of basal (cytokeratin 5 CK5; p63), luminal (cytokeratin 8, CK8; androgen receptor, AR), and neuroendocrine cells (synaptophysin) were detected. Representative single channel and merged images for all antibodies used are presented together with negative control (staining with secondary antibodies only). Representative results from five independent repetitions are shown. Images were acquired on a confocal microscope Olympus FV10i using 60× obj. with zoom 2×. Scale bar 50 μm, scale bar in inset 20 μm.

Trop-2$^+$ cells residing in adult mouse prostate possess partial mesenchymal traits with elevated levels of EMT regulator *Snai2/*Slug. Functionally, the Slug-expressing cells are capable of forming organoids containing all prostate epithelial cells – basal, luminal, and neuroendocrine.

Declaration of Competing Interest

The authors declare that they have no known competing financial interests or personal relationships that could have appeared to influence the work reported in this paper.

C)

Fig. 5. (*continued*)

Appendix A. Supplementary data

Supplementary data to this article can be found online at https://doi.org/10.1016/j.scr.2020.101844.

References

Lee, D.K., Liu, Y., Liao, L., Wang, F., Xu, J., 2014. The prostate basal cell (BC) heterogeneity and the p63-positive BC differentiation spectrum in mice. Int. J. Biol. Sci. 10, 1007–1017.

Zhou, J., Feigenbaum, L., Yee, C., Song, H., Yates, C., 2013. Mouse prostate epithelial luminal cells lineage originate in the basal layer where the primitive stem/early progenitor cells reside: implications for identifying prostate cancer stem cells. Biomed. Res. Int. 2013, 913179.

Goldstein, A.S., Lawson, D.A., Cheng, D., Sun, W., Garraway, I.P., Witte, O.N., 2008. Trop2 identifies a subpopulation of murine and human prostate basal cells with stem cell characteristics. Proc. Natl. Acad. Sci. U.S.A. 105, 20882–20887.

Stoyanova, T., Goldstein, A.S., Cai, H., Drake, J.M., Huang, J., Witte, O.N., 2012. Regulated proteolysis of Trop2 drives epithelial hyperplasia and stem cell self-renewal via beta-catenin signaling. Genes Dev. 26, 2271–2285.

Bonkhoff, H., Remberger, K., 1996. Differentiation pathways and histogenetic aspects of normal and abnormal prostatic growth: a stem cell model. Prostate 28, 98–106.

Szczyrba, J., Niesen, A., Wagner, M., Wandernoth, P.M., Aumuller, G., Wennemuth, G., 2017. Neuroendocrine cells of the prostate derive from the neural crest. J. Biol. Chem. 292, 2021–2031.

Karthaus, W.R., Iaquinta, P.J., Drost, J., Gracanin, A., van Boxtel, R., Wongvipat, J., Dowling, C.M., Gao, D., Begthel, H., Sachs, N., Vries, R.G., Cuppen, E., Chen, Y., Sawyers, C.L., Clevers, H.C., 2014. Identification of multipotent luminal progenitor cells in human prostate organoid cultures. Cell 159, 163–175.

Zhang, Y., Weinberg, R.A., 2018. Epithelial-to-mesenchymal transition in cancer: complexity and opportunities. Front. Med. 12, 361–373.

Lamouille, S., Xu, J., Derynck, R., 2014. Molecular mechanisms of epithelial-mesenchymal transition. Nat. Rev. Mol. Cell. Biol. 15, 178–196.

Lukacs, R.U., Goldstein, A.S., Lawson, D.A., Cheng, D., Witte, O.N., 2010. Isolation, cultivation and characterization of adult murine prostate stem cells. Nat. Protoc. 5, 702–713.

Ye, X., Tam, W.L., Shibue, T., Kaygusuz, Y., Reinhardt, F., Ng Eaton, E., Weinberg, R.A., 2015. Distinct EMT programs control normal mammary stem cells and tumour-initiating cells. Nature 525, 256–260.

Spidlen, J., Breuer, K., Rosenberg, C., Kotecha, N., Brinkman, R.R., 2012. FlowRepository: a resource of annotated flow cytometry datasets associated with peer-reviewed publications. Cytometry A 81, 727–731.

Drost, J., Karthaus, W.R., Gao, D., Driehuis, E., Sawyers, C.L., Chen, Y., Clevers, H., 2016. Organoid culture systems for prostate epithelial and cancer tissue. Nat. Protoc. 11, 347–358.

Schindelin, J., Arganda-Carreras, I., Frise, E., Kaynig, V., Longair, M., Pietzsch, T., Preibisch, S., Rueden, C., Saalfeld, S., Schmid, B., Tinevez, J.Y., White, D.J., Hartenstein, V., Eliceiri, K., Tomancak, P., Cardona, A., 2012. Fiji: an open-source platform for biological-image analysis. Nat. Methods 9, 676–682.

Livak, K.J., Schmittgen, T.D., 2001. Analysis of relative gene expression data using real-time quantitative PCR and the 2(-Delta Delta C(T)) Method. Methods 25, 402–408.

Leong, K.G., Wang, B.E., Johnson, L., Gao, W.Q., 2008. Generation of a prostate from a single adult stem cell. Nature 456, 804–808.

Mani, S.A., Guo, W., Liao, M.J., Eaton, E.N., Ayyanan, A., Zhou, A.Y., Brooks, M., Reinhard, F., Zhang, C.C., Shipitsin, M., Campbell, L.L., Polyak, K., Brisken, C., Yang, J., Weinberg, R.A., 2008. The epithelial-mesenchymal transition generates cells with properties of stem cells. Cell 133, 704–715.

Kong, D., Banerjee, S., Ahmad, A., Li, Y., Wang, Z., Sethi, S., Sarkar, F.H., 2010. Epithelial to mesenchymal transition is mechanistically linked with stem cell signatures in prostate cancer cells. PLoS One 5, e12445.

Grant, C.M., Kyprianou, N., 2013. Epithelial mesenchymal transition (EMT) in prostate growth and tumor progression. Transl. Androl. Urol. 2, 202–211.

Nieto, M.A., Huang, R.Y., Jackson, R.A., Thiery, J.P., 2016. Emt: 2016. Cell 166, 21–45.

Futterman, M.A., Garcia, A.J., Zamir, E.A., 2011. Evidence for partial epithelial-to-mesenchymal transition (pEMT) and recruitment of motile blastoderm edge cells during avian epiboly. Dev. Dyn. 240, 1502–1511.

Grigore, A.D., Jolly, M.K., Jia, D., Farach-Carson, M.C., Levine, H., 2016. Tumor budding: the name is EMT. Partial EMT. J. Clin. Med. 5.

Yu, M., Bardia, A., Wittner, B.S., Stott, S.L., Smas, M.E., Ting, D.T., Isakoff, S.J., Ciciliano, J.C., Wells, M.N., Shah, A.M., Concannon, K.F., Donaldson, M.C., Sequist, L.V., Brachtel, E., Sgroi, D., Baselga, J., Ramaswamy, S., Toner, M., Haber, D.A., Maheswaran, S., 2013. Circulating breast tumor cells exhibit dynamic changes in epithelial and mesenchymal composition. Science 339, 580–584.

Hu, W.Y., Hu, D.P., Xie, L., Li, Y., Majumdar, S., Nonn, L., Hu, H., Shioda, T., Prins, G.S., 2017. Isolation and functional interrogation of adult human prostate epithelial stem cells at single cell resolution. Stem Cell Res. 23, 1–12.

Signoretti, S., Waltregny, D., Dilks, J., Isaac, B., Lin, D., Garraway, L., Yang, A., Montironi, R., McKeon, F., Loda, M., 2000. p63 is a prostate basal cell marker and is required for prostate development. Am. J. Pathol. 157, 1769–1775.

Bolos, V., Peinado, H., Perez-Moreno, M.A., Fraga, M.F., Esteller, M., Cano, A., 2003. The transcription factor slug represses e-cadherin expression and induces epithelial to mesenchymal transitions: a comparison with Snail and E47 repressors. J. Cell Sci. 116, 499–511.

Guo, W., Keckesova, Z., Donaher, J.L., Shibue, T., Tischler, V., Reinhardt, F., Itzkovitz, S., Noske, A., Zurrer-Hardi, U., Bell, G., Tam, W.L., Mani, S.A., van Oudenaarden, A., Weinberg, R.A., 2012. Slug and Sox9 cooperatively determine the mammary stem cell state. Cell 148, 1015–1028.

Zhang, D., Park, D., Zhong, Y., Lu, Y., Rycaj, K., Gong, S., Chen, X., Liu, X., Chao, H.P., Whitney, P., Calhoun-Davis, T., Takata, Y., Shen, J., Iyer, V.R., Tang, D.G., 2016. Stem cell and neurogenic gene-expression profiles link prostate basal cells to aggressive prostate cancer. Nat. Commun. 7, 10798.

Nassour, M., Idoux-Gillet, Y., Selmi, A., Come, C., Faraldo, M.L., Deugnier, M.A., Savagner, P., 2012. Slug controls stem/progenitor cell growth dynamics during mammary gland morphogenesis. PLoS One 7, e53498.

Fatehullah, A., Tan, S.H., Barker, N., 2016. Organoids as an in vitro model of human development and disease. Nat. Cell Biol. 18, 246–254.